

## COMPUTATIONAL MODELS FOR NANOSECOND LASER ABLATION

HARIHAR KHANAL<sup>1</sup>, DAVID AUTRIQUE<sup>2</sup>, AND VASILIOS ALEXIADES<sup>3</sup>

<sup>1</sup>Department of Mathematics, Embry-Riddle Aeronautical University  
Daytona Beach, FL 32114, USA.

<sup>2</sup>Department of Physics, Optimas Research Center - TU Kaiserslautern  
67653 Kaiserslautern, Germany.

<sup>3</sup>Department of Mathematics, University of Tennessee, Knoxville, TN 37996, USA.

*Corresponding author: Harihar Khanal (harihar.khanal@erau.edu)*

**ABSTRACT.** Laser ablation in an ambient environment is becoming increasingly important in science and technology. It is used in applications ranging from chemical analysis via mass spectroscopy, to pulsed laser deposition and nanoparticle manufacturing. We describe numerical schemes for a multiphase hydrodynamic model of nanosecond laser ablation expressing energy, momentum, and mass conservation in the target material, as well as in the expanding plasma plume, along with collisional and radiative processes for laser-induced breakdown (plasma formation). Numerical simulations for copper in a helium background gas are presented and the efficiency of various ODE integrators is compared.

**AMS (MOS) Subject Classification.** 35Q35, 65Z05.

### 1. INTRODUCTION

Laser ablation is the process of mass removal from a sample by delivering laser energy to a target material. Laser ablation is used in a variety of medical, scientific and industrial applications, such as surgery, chemical analysis, laser machining, etc, [7, 11, 25, 26].

During the last three decades, there have been significant attempts to investigate the interaction of nanosecond pulsed lasers with solid targets and to study the properties of laser-produced plasmas using various computational approaches: kinetic models [21, 18, 13], hydrodynamic models [29, 1, 15, 22, 6, 3, 9, 27, 32, 24, 12, 2, 5], and hybrid models such as [14, 17].

In this paper, we use a multiphase hydrodynamic model, described in [4] and [19], which accounts for target heating, surface and volumetric mass removal, as well as plume expansion and plasma formation. The model consists of a tightly coupled system of partial differential equations (describing conservation of mass, momentum

and energy) and ordinary differential equations (describing collisional and radiative processes). This is a computationally intensive problem demanding efficient numerical algorithms [19].

In our previous work [19], about a dozen (explicit) ODEs integrators including adaptive Runge-Kutta-Fehlberg (RKFB4), Dormand-Prince (DoPri5), and high order explicit PEER methods [31] (up to 9th order) were tested and compared for their efficiency (CPU timings). The simulation results showed that the higher order accuracy of high order schemes did not translate to speedup, as we had to use very fine step size to maintain accuracy. It raised a question on the effectiveness of explicit schemes. Is the system really so stiff that it requires specific efficient solution methods?

As such, we performed further tests exploring other solvers for stiff systems (multistep and jacobian free implicit schemes) and improved the coding strategy.

This paper extends the authors' previous work [19] by including solvers from two other packages for the ODE system: Intel DODE, and VODE.

The simulation results show that lower order methods are much faster than higher order for our model problem. Surprisingly, the stiff methods performed worse than non-stiff, indicating that our ODE system is not as stiff as we thought.

Here we will focus on the efficiency of numerical schemes. As such, various ODE integration methods will be compared.

The paper is organized as follows. After outlining the highlights of the employed modeling procedure, we present the mathematical model of laser ablation in §2. The computational approach is described in §3 and some simulation results are presented in §4, with conclusions in §5.

## 2. LASER ABLATION MODEL

Laser ablation is characterized by several strongly coupled physical and chemical processes occurring in and above the solid target.

The main processes can be summarized as follows: the solid target heats up, a thin layer melts and finally the melt vaporizes. The vapor plume will interact with the impinging laser light, resulting in a hot plasma that quickly expands above the target surface. Accordingly, the ablation process involves

- Heat conduction, melting and surface evaporation below the critical temperature;
- A Knudsen transition layer connecting target and plume;
- Volumetric mass removal at the critical temperature;
- Plasma formation, expansion, laser absorption by the plume, shielding of target, recondensation in the plume.

**2.1. Target Heating.** During the initial stage of ns-laser ablation, part of the laser energy is absorbed near the target surface. The latter is converted into heat, that conducts through the solid target, causing melting and removal (ablation) of some of the target material. Target heating is described by the simultaneous solution of an internal energy equation, continuity equation and a pressure relaxation equation, in a coordinate system attached to the ablating surface (moving with speed  $v_{rec}$ , which is one of the unknowns).

$$(2.1) \quad \frac{\partial U}{\partial t} - v_{rec}(t) \frac{\partial U}{\partial x} = \frac{\partial}{\partial x} k(T) \frac{\partial T}{\partial x} + S_{las}(x, t) .$$

$$(2.2) \quad \frac{\partial \rho}{\partial t} - v_{rec}(t) \frac{\partial \rho}{\partial x} = - \frac{\partial \rho v}{\partial x} .$$

$$(2.3) \quad \frac{\partial P_m}{\partial t} - v_{rec}(t) \frac{\partial P_m}{\partial x} = - \frac{P_m - P_{amb}}{\tau_{mech}} .$$

Here  $U$  denotes the internal energy density,  $v_{rec}$  is the surface recession velocity,  $\kappa(T)$  is the temperature dependent thermal conductivity,  $\rho$  is mass density,  $v$  is material velocity.  $P_m$  and  $P_{amb}$  denote the material and ambient pressure,  $\tau_{mech}$  expresses the mechanical relaxation time ( $\tau_{mech}(x, t) = x/c_{snd}(x, t)$ , where  $x$  and  $c_{snd}$  are the spatial coordinate and the local speed of sound in the target).

The laser source term  $S_{las}$  in (2.1) is given by:

$$(2.4) \quad S_{las}(x, t) = \beta I_{max} e^{-(t-t_{max})^2/2\sigma^2} (1 - R) \alpha e^{-\alpha x} ,$$

where  $R(T)$  and  $\alpha(T)$  denote the reflection and absorption coefficients of the target respectively,  $I_{max}$  denotes the maximum intensity (input parameter, see §4.1), whereas  $\beta$  represents the total shielding coefficient at the target surface that depends on the laser wavelength, plume temperature as well as on the species densities (neutrals, ions and electrons) above the target.

The system of equations (2.1-2.3) is closed by a multiphase equation of state (EOS) [23].

**2.2. Knudsen Layer.** Above the target, the evaporated particles achieve translational equilibrium within a few mean free paths by means of collisions, in a thin zone, known as the *Knudsen layer* (KL) [7]. The Knudsen layer provides the connection between the target and the plasma plume.

In this region  $T$ ,  $P$ ,  $\rho$ ,  $v$  undergo jumps governed by the local Mach number  $M$ . We use Knight's relations [20] for vaporization into a background gas:

$$(2.5) \quad \frac{T_K}{T_s} = \left[ \sqrt{1 + \pi \left( \frac{m}{2} \left( \frac{\gamma - 1}{\gamma + 1} \right) \right)^2} - \sqrt{\pi} \frac{m}{2} \left( \frac{\gamma - 1}{\gamma + 1} \right) \right]^2 ,$$

$$(2.6) \quad \frac{P_K}{P_s} = \sqrt{\frac{T_K}{T_s}} \left[ \left( m^2 + \frac{1}{2} \right) e^{m^2} \operatorname{erfc}(m) - \frac{m}{\sqrt{\pi}} \right] + \frac{1}{2} \left[ 1 - \sqrt{\pi} e^{m^2} \operatorname{erfc}(m) \right],$$

$$(2.7) \quad m = \frac{v_K}{\sqrt{2RT_K}}, \quad M = \frac{v_K}{\sqrt{\gamma RT_K}}.$$

$P_K/P_s \leq 1$  for vaporization ( $M \geq 0$ ), else  $P_K/P_s = 0.95e^{2.42|M|} > 1$  for condensation ( $M < 0$ ).

**2.3. Vapor Flow.** Beyond the Knudsen layer, the dense vapor plume ionizes during the laser action. A plasma is formed that absorbs laser energy, thus shielding the target surface from the incoming laser light. The absorption of laser energy by the plasma results in very high plume temperatures, velocities, species densities, pressures, etc. Afterwards, this hot plasma quickly expands into the ambient environment. The expanding plume is modeled by a set of compressible Euler equations and closed by a multiphase equation of state (EOS) [4].

$$(2.8) \quad \frac{\partial \rho}{\partial t} = -\frac{\partial \rho v}{\partial x}$$

$$(2.9) \quad \frac{\partial \rho_v}{\partial t} = -\frac{\partial \rho_v v}{\partial x}$$

$$(2.10) \quad \frac{\partial \rho v}{\partial t} = -\frac{\partial}{\partial x} \left( \rho v^2 + P + \frac{\partial}{\partial x} \tau_{xx} \right)$$

$$(2.11) \quad \frac{\partial \rho \varepsilon}{\partial t} = -\frac{\partial (\rho \varepsilon + P) v}{\partial x} - \frac{\partial}{\partial x} (q + \tau_{xx}) + S_{IB} + S_{MPI} - S_{rad}$$

These equations express mass (2.8), momentum (2.9), and energy conservation (2.10) in the plume domain. Here  $\rho = \rho_v + \rho_b$  denotes the total mass density, with  $\rho_v$  and  $\rho_b$  the partial densities of vapor and background gas, respectively. The total momentum density and the total energy density are given by  $\rho v$  and  $\rho \varepsilon$  respectively.  $P$  denotes the total pressure, whereas  $q$  is the heat flux transported by the various species in the plasma. The source terms  $S_{IB}$  (due to inverse Bremsstrahlung),  $S_{(M)PI}$  (due to photon ionization) and  $S_{rad}$  (radiation loss of the plasma) encountered in the energy equation (2.11) are provided by a collisional radiative model describing optical breakdown in the plasma [33].

**2.4. Laser Induced Breakdown.** In the irradiated vapor several collisional and radiative processes take place. The laser will trigger breakdown in the dense expanding vapor formed above the target surface. Laser induced breakdown is modeled by a highly nonlinear system of ODEs (collisional radiative model) [19] describing:

- single- and multi-photon ionization,
- radiative decay electron impact excitation and ionization,
- respective recombination reactions, inverse Bremsstrahlung.

Collecting the  $n$  unknowns into a vector  $y \in \mathbb{R}^n$ , and the coefficients/parameters into a vector  $p \in \mathbb{R}^m$ , a concise (computational) representation of the collisional radiative model takes the form of a system of  $n$  first order ODEs containing  $m$  parameters.

$$(2.12) \quad \frac{dy}{dt} = f(t, y(t, p), p), \quad 0 < t \leq t_{max}, \quad y \in \mathbb{R}^n, \quad p \in \mathbb{R}^m$$

where  $y$  is an array containing the number densities of ions, electrons, excited states and their energies;  $p$  is an array of parameters of the model, that contains all the rate constants (which depend on the temperature, density and spectroscopic properties of the species). We note that

- The ODE system (2.12) can be solved numerically by any ODE integrator, and we tried several.
- Evaluation of the right hand side function  $f(t, y(t, p), p)$  is very expensive.

When the plume reaches a state close to Local Thermodynamic Equilibrium (LTE), the atomic levels become Boltzmann distributed and a local state is achieved where electrons, ions, and their excited states are characterized by the same temperature  $T$ . At that instant the plasma is described in the ideal gas approximation and the temperature, electron and ion densities are obtained from the Saha equation [33], [4].

### 3. COMPUTATIONAL APPROACH

The system of PDEs (2.1–2.3) for the target and (2.8–2.11) for the plume are approximated by an explicit Finite Volume method. The system of ODEs describing the collisional radiative process in the plasma (2.12) is solved using several ODE integrators including, Intel ODE [16] and VODE [10] solvers.

**3.1. Finite Volume for Conservation Laws.** We write the mathematical model described by the conservation laws in divergence form as

$$(3.1) \quad \frac{\partial \mathcal{U}}{\partial t} + \nabla \cdot \vec{\mathcal{F}}(\mathcal{U}) = \mathcal{S}(\mathcal{U})$$

Here  $\mathcal{U}$  is a conserved quantity (per unit volume),  $\vec{\mathcal{F}}$  is the total flux (amount crossing a unit area per unit time), and  $\mathcal{S}$  is the source density (per unit volume per unit time).

**Spatial Discretization.** We partition the computational domain into  $M$  control volumes  $V_i = (x_{i-\frac{1}{2}}, x_{i+\frac{1}{2}})$  centered at  $x_i$ ,  $i = 1, \dots, M$ . Let  $\Delta x_i$  denote the length of the cell. Integration of (3.1) over each control volume  $V_i$  yields the following semi-discrete scheme.

$$(3.2) \quad \begin{cases} \frac{d}{dt} U_i = \mathcal{S}_i(t) - \frac{1}{\Delta x_i} \left( \mathcal{F}_{i+\frac{1}{2}} - \mathcal{F}_{i-\frac{1}{2}} \right) \\ U_i(0) = \frac{1}{\Delta x_i} \int_{V_i} \mathcal{U}(x, 0) dx \end{cases}$$

Here  $U_i(t)$  and  $S_i(t)$  are cell average of  $\mathcal{U}(x, t)$  and  $\mathcal{S}(x, t)$  on the  $i$ -th control volume, and  $\mathcal{F}_{i\pm\frac{1}{2}}$  are the numerical approximation to the fluxes on the cell faces.

To resolve the strong temperature and pressure gradients and capture shock waves, special attention is given in the spatial discretization of (3.1). More specifically, we employed a non-uniform fine grid in the target, with a high nodal density near the surface, whereas an adaptive grid was applied[30] while solving the Euler equations (2.8–2.11) in the plume.

**Fully Discrete Model.** Keeping future parallelization in mind, the initial value problem of the ODE system (3.2) is discretized in time using the forward Euler method. Let  $\Delta t_n$  be the temporal variable step-size and let  $t^{n+1} = t^n + \Delta t_n, n \geq 0$  be the discrete time levels, then the fully discrete finite volume scheme for the conservation laws (3.1) takes the form

$$(3.3) \quad U_i^{n+1} = U_i^n + \frac{\Delta t_n}{\Delta x_i} \left( \mathcal{F}_{i-\frac{1}{2}}^n - \mathcal{F}_{i+\frac{1}{2}}^n \right) + \Delta t_n S_i^n, \quad i = 1, \dots, M.$$

The numerical scheme (3.3) is very simple to implement but it has a severe restriction on time step size (CFL condition for stability).

In order to save computational time, an adaptive grid is used to solve the Euler equations (2.8–2.11) during the plume expansion [30]. The grid expands ahead of the heat wave in the target domain and ahead of the expanding plasma in the plume domain. The increment in the grid points is determined by the height  $H$  of the plume, which is approximated by integrating the speed of sound  $H = \int a(t) dt$ .

**3.2. ODE Integrators for Collisional Radiative Model.** The collisional radiative model (2.12) has to be solved simultaneously with the system of PDEs (2.1–2.11) that accounts for target heating and vapor flow. In our simulations there are  $n = 62$  ODEs in the system and  $m = 4$  parameters passed through the right hand side function.

The ODE system contains various fast scales and requires smaller time-step than the PDEs. We use  $\Delta t_{ODE} = \Delta t_{CFL}/factor$ , and report the *factor* used by each solver. In our computations, stepsize  $\Delta t_{ODE}$  becomes as small as  $10^{-15}$ s.

We have implemented and tested various numerical methods for the ODE system (2.12). Here we briefly describe only the Intel ODE and VODE packages. A description of the other methods and their respective implementation aspects appear in our earlier work [19].

- The Intel ODE library [16] offers explicit, implicit, and mixed solvers for non-stiff and stiff problems as well as for problems with variable stiffness. It contains three types of solvers (labeled as dode a, b, c in Table 1):

- *rk45*: explicit Merson 4th order multi-stage solver with extended stability domains for non-stiff and middle-stiff ODE problems.
- *lsode*: implicit L-stable(5,2) solver for stiff ODEs.
- *dodesol*: all-purpose hybrid solver for problems with unknown or variable stiffness, with automatic choice of integration method.
- VODE [10] is a suite of multistep-based ODE solvers for non-stiff and stiff systems. It uses high order variable-coefficient Adams-Moulton and Backward Differentiation Formula (BDF) methods in Nordsieck form. It controls stability and accuracy by varying the time-step and the order of the integrator. We used the Fortran 90 extension [10] of the venerable f77 DVODE.f code [8] and employed the following four solvers of DVODE.F90:
  - MF=10: implicit Adams method up to order 12, with functional iteration (no Jacobian).
  - MF=12: implicit Adams method up to order 12, with internally generated (difference quotient) full Jacobian.
  - MF=20: stiff BDF method up to order 5 with functional iteration (no Jacobian).
  - MF=22: stiff BDF method up to order 5 with internally generated full Jacobian.

## 4. NUMERICAL RESULTS

**4.1. Simulation Setup.** We present simulations for ns laser ablation of copper (Cu) in a helium (He) background gas. The target thickness is  $12\mu m$ . The laser has a wavelength of 532 nm and a pulse width of 6 ns. Initially, both target and background gas are in a stationary state at standard temperature (300 K) and pressure (1 atm). Simulations are carried out up to time  $t_{max} = 50ns$ , well beyond the duration of a single laser pulse, for intensity  $I_0 = 12.e12 W/m^2$ , and wave length  $\lambda = 532 nm$ .

The numerical code is written in Fortran 90, compiled with Intel Fortran, and ran on Xeon-class processors (AMD Opteron 2378, 2400 MHz, 512 KB cache).

**4.2. Grid Convergence.** In the simulations reported here, we employ a fairly fine non-uniform grid consisting of 2000 control volumes along the direction of laser beam (denser near the surface). The smallest target cells (of size  $\Delta x = 6nm$ ) are placed in the near-surface region. In the plume regions  $\Delta x = 500nm$ , adaptively refined till the grid reaches a lower limit of  $\Delta x = 50nm$ . Finer grids were tested, with no discernible effect (to at least 3 significant digits).

Variable time-stepping is employed respecting the CFL condition in the entire computational domain. Time steps are of order  $10^{-13}$  s. To solve the ODE system

for the breakdown process,  $\Delta t$  is divided by a factor of up to 500, depending on the scheme.

**4.3. Numerical Experiments.** We tested the following 17 numerical schemes for the ODE system (2.12):

- Explicit Euler (with time step factors 50 and 100)
- Explicit RK2, RK3, RK4, RKFB4, DoPri5 (2nd, 3rd and 4th order Runge-Kutta methods, adaptive 4th order Runge-Kutta-Fehlberg, 5th order Dormand-Prince)
- Explicit PEER (adaptive) of orders 7,8,9 (two-step peer methods with automatic step size control [28])
- Intel ODE solvers *rkm9st*, *mk52lfn*, *dodesol* (adaptive, high order), described earlier.
- VODE (variable order, adaptive) Adams:10,12, BDF:20,22

Comparison of performance of all the time-steppers employed is presented in Table 1 and displayed in Fig. 1 and Fig. 2.

All solvers produced essentially identical-looking plots, with the exception of RKFB4 and DoPri5 which failed to produce acceptable accuracy (their timings are shown in parentheses). The time step factor, mentioned in §3.2, is listed in Table 1. Only the VODE solvers can use factor=10, RK4 can use factor=40, explicit Euler factor=50, all others require factor  $\geq 100$ , i.e. smaller time-steps. We could not improve this factor by using higher order and adaptive time steppers, contrary to our expectations.

Explicit Euler turns out to be the fastest solver. Moreover, fixed step size schemes perform better than the adaptive ones.

## 5. CONCLUSION

In this paper we outlined a mathematical model of ns-laser ablation process based on a multiphase hydrodynamic model coupled to a collisional radiative model, and presented computational models employing several time stepping schemes. Next, we compared the performance of 17 ODE integrators for ns-laser ablation of a copper target in helium background gas with laser wavelength of 532 nm and peak intensity  $10^{13}$  W/m<sup>2</sup>. All solvers produce identical plots (agree by eye-norm), except rkfb4 and DoPri5 which failed (we had to relax TOL and their plots are off).

A summary of the main findings on the comparison of the 17 time steppers employed here on the collisional radiative model is as follows.

- The lower order methods are much faster than higher order. The cost of evaluation of right hand side functions in the ODE system is very high, so the fewer the better.

TABLE 1. CPU timings of 17 ODE solvers for 50ns runs with  $I_o = 12.e12 \text{ W/m}^2$ ,  $\lambda = 532 \text{ nm}$ .

time-stepper	factor	cpu (sec)	cpu (min)	comments
EE	50	2248	<b>37</b>	<b>best!</b>
EE	100	2466	41	
RK2	50	3124	52	
RK3	50	3451	58	
RK4	40	2985	50	
RKFB4	400	(4075)	(70)	inaccurate
DoPri5	500	(4610)	(77)	inaccurate
Peer 7	100	35643	594	
Peer 8	100	38869	648	
Peer 9	100	46143	769	
dode a	100	5144	86	
dode b	100	5806	97	
dode c	100	51717	862	worst
VODE 10	10	2766	46	<b>2nd best</b>
VODE 12	10	8490	142	
VODE 20	10	2823	47	<b>3rd best</b>
VODE 22	10	8748	146	

- The non-adaptive methods performed better than adaptive.
- The non-stiff methods performed better than the stiff, indicating that our ODE system may not be as stiff as we thought, or at least it does not behave as stiff.
- None of the sophisticated methods could beat explicit Euler, contrary to what numerical analysis texts typically suggest.
- The undisputed winner is Explicit Euler, next come vode10 (24% slower), vode20 (27% slower), rk4 (35% slower).

The numerical experiments on the ODE system for the collisional radiative model lead to the conclusion that the higher accuracy of high order schemes does not always translate to computational efficiency in practice. This is likely here due to the very high cost of evaluating the right hand side of the ODEs, and the fine space (and time) steps necessary for accuracy.

Analytically computed Jacobians may improve performance of some of the implicit solvers that are currently implemented with internally generated Jacobians. For overall efficiency of the computational model further tests are under way, exploring implicit solvers with exact Jacobians, strongly stable higher order methods for the

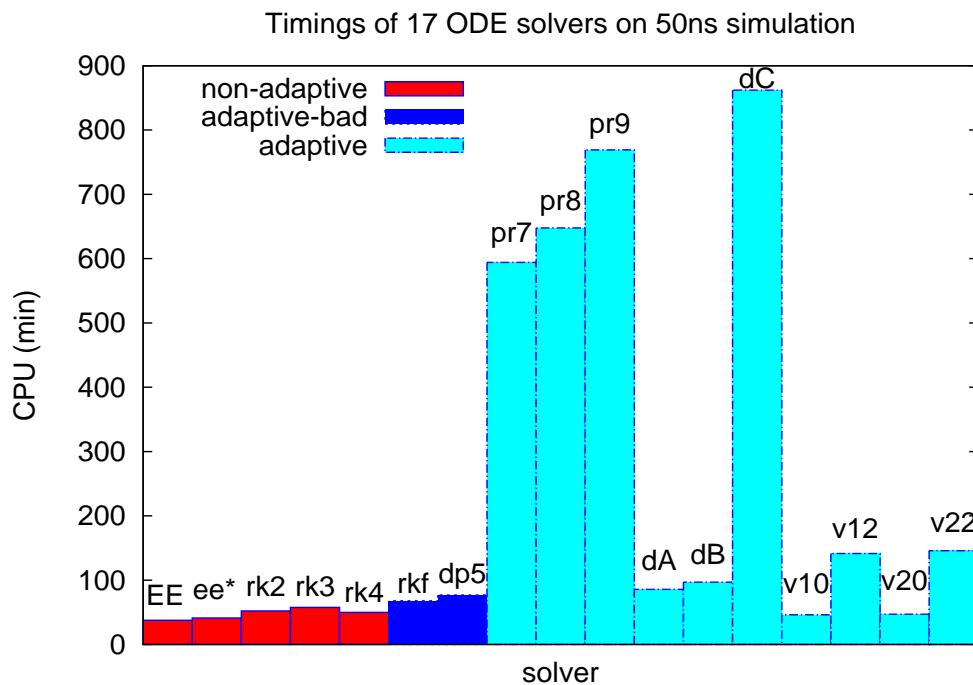


FIGURE 1. Timings of 17 ODE solvers on 50ns simulation

conservation laws, and high performance computing strategies through (CPU/GPU) parallelization.

## ACKNOWLEDGMENTS

The first author (HK) would like to thank the Department of Mathematics and the Office of Sponsored Research, Embry-Riddle Aeronautical University for support.

## REFERENCES

1. M. Aden, E.W. Kreutz, and A. Voss, *Laser-induced plasma formation during pulsed laser deposition*, Journal of Physics D: Applied Physics **26** (1993), 1545–1553.
2. V. Alexiades and D. Autrique, *Enthalpy model for heating, melting, and vaporization in laser ablation*, Electronic Journal of Differential Equations **Conf. 19** (2010), 1–14.
3. S.I. Anisimov and B.S. Luk'yanchuk, *Selected problems of laser ablation theory*, Physics-Uspekhi **45** (2002), no. 3, 293–324.
4. D. Autrique, V. Alexiades, and H. Khanal, *Hydrodynamic modeling of ns-laser ablation*, Electronic Journal of Differential equations **Conf. 20** (2013), 1–14.

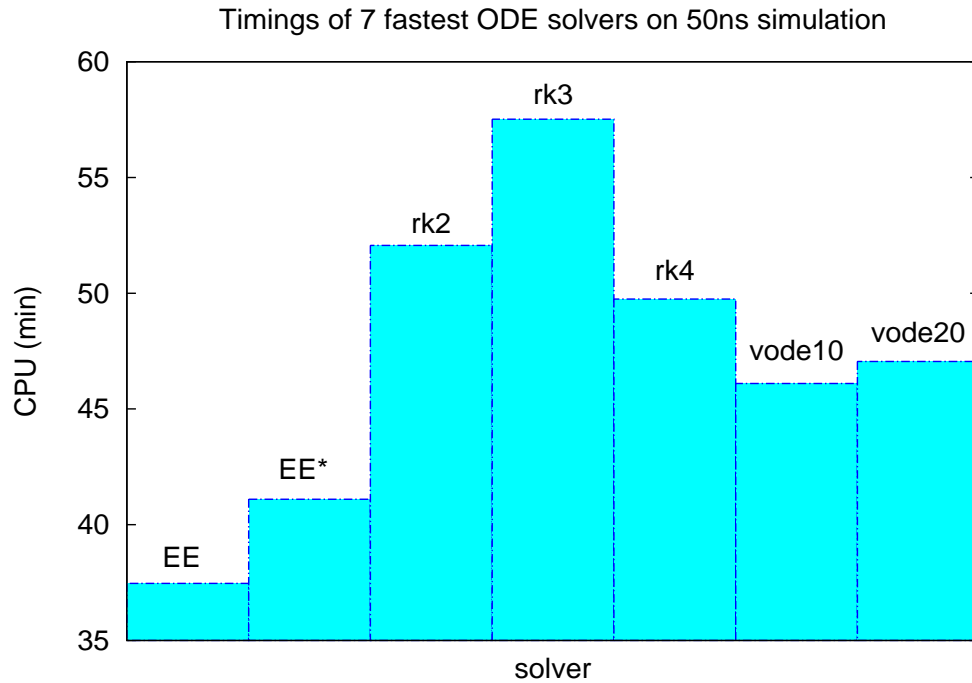


FIGURE 2. Timings of the 7 best ODE solvers on 50ns simulation

5. D. Autrique, Z. Chen, V. Alexiades, A. Bogaerts, and B. Rethfeld, *A multiphase model for pulsed ns-laser ablation of copper in an ambient gas*, AIP Conference Proceedings, vol. 1464, 2012, p. 648.
6. L. Balazs, R. Gijbels, and A. Vertes, *Expansion of laser-generated plumes near the plasma ignition threshold*, Analytical chemistry **63** (1991), no. 4, 314–320.
7. D. Bäuerle, *Laser Processing and Chemistry*, Springer Verlag, Berlin, 2011.
8. P.N. Brown, G.D. Byrne, and A.C. Hindmarsh, *vode.f*, 1989–2002, <http://www.netlib.org/ode/vode.f>.
9. A.V. Bulgakov and N.M. Bulgakova, *Dynamics of laser-induced plume expansion into an ambient gas during film deposition*, Journal of physics D: applied physics **28** (1995), no. 8, 1710–1718.
10. G.D. Byrne and S. Thompson, *A fortran 90 extension of the f77 dvode.f code*, 2008, <http://www.radford.edu/~thompson/vodef90web/>.
11. D.B. Chrisey and G.K. Hubler, *Pulsed Laser Deposition of Thin Films*, Wiley, New York, 1994.
12. G. Clair and D. L'Hermite, *1D modelling of nanosecond laser ablation of copper samples in argon at  $P = 1$  atm with a wavelength of 532 nm*, Journal of Applied Physics **110** (2011), no. 8, 083307.
13. F. Garrelie, C. Champeaux, and A. Catherinot, *Study by a Monte Carlo simulation of the influence of a background gas on the expansion dynamics of a laser-induced plasma plume*, Applied Physics A: Materials Science & Processing **69** (1999), no. 1, 45–50.

14. S.S. Harilal, C.V. Bindhu, M.S. Tillack, F. Najmabadi, and A.C. Gaeris, *Internal structure and expansion dynamics of laser ablation plumes into ambient gases*, Journal of Applied Physics **93** (2003), no. 5, 2380–2388.
15. J.R. Ho, C.P. Grigoropoulos, and J.A.C. Humphrey, *Computational study of heat transfer and gas dynamics in the pulsed laser evaporation of metals*, Journal of Applied Physics **78** (1995), no. 7, 4696–4709.
16. Y. Laevsky (Intel), *Intel ordinary differential equations solver library*, 2011, <https://software.intel.com/en-us/articles/intel-ordinary-differential-equations-solver-library>.
17. T.E. Itina, J. Hermann, P. Delaporte, and M. Sentis, *Laser-generated plasma plume expansion: Combined continuous-microscopic modeling*, Physical Review E **66** (2002), no. 6, 066406.
18. T.E. Itina, V.N. Tokarev, W. Marine, and M. Autric, *Monte Carlo simulation study of the effects of nonequilibrium chemical reactions during pulsed laser desorption*, Journal of Chemical Physics **106** (1997), no. 21, 8905–8912.
19. H. Khanal, D. Autrique, and V. Alexiades, *Time-stepping for laser ablation*, Electronic Journal of Differential equations **Conf. 20** (2013), 93–101.
20. C.J. Knight, *Theoretical modeling of rapid surface vaporization with back pressure*, AIAA journal **17** (1979), no. 5, 519–523.
21. J.C.S. Kools, *Monte Carlo simulations of the transport of laser-ablated atoms in a diluted gas*, Journal of Applied Physics **74** (1993), no. 10, 6401–6406.
22. H.C. Le, D.E. Zeitoun, J.D. Parisse, M. Sentis, and W. Marine, *Modeling of gas dynamics for a laser-generated plasma: Propagation into low-pressure gases*, Physical Review E **62** (2000), no. 3 Pt B, 4152–4161.
23. P.R. Levashov and K.V. Khishchenko, *Itteos 5.8 software for calculation of eos for metals*, 2007.
24. V.I. Mazhukin, V.V. Nossov, and I. Smurov, *Modeling of plasma-controlled evaporation and surface condensation of Al induced by 1.06 and 0.248  $\mu$ m laser radiations*, Journal of Applied Physics **101** (2007), no. 2, 024922–024922.
25. J.C. Miller and R.F. Haglund, *Laser ablation and desorption*, Academic Press, New York, 1998.
26. A. Montaser, *Inductively Coupled Plasma Mass Spectrometry*, Wiley, New York, 1998.
27. M.S. Qaisar and G.J. Pert, *Laser ablation of Mg, Cu, and Pb using infrared and ultraviolet low-fluence lasers*, Journal of Applied Physics **94** (2003), no. 3, 1468–1477.
28. B.A. Schmitt and R. Weiner, *Manual for the Explicit Parallel Peer Code EPPEER*, 2012, <http://www.mathematik.uni-marburg.de/~schmitt/peer>.
29. R.K. Singh and J. Narayan, *Pulsed-laser evaporation technique for deposition of thin films: Physics and theoretical model*, Physical Review B **41** (1990), no. 13, 8843–8859.
30. H. Tang and T. Tang, *Adaptive mesh methods for one-and two-dimensional hyperbolic conservation laws*, SIAM Journal on Numerical Analysis **41** (2003), no. 2, 487–515.
31. R. Weiner, K. Biermann, B.A. Schmitt, and H. Podhaisky, *Explicit two-step peer methods*, Computers & Mathematics with Applications **55** (2008), no. 4, 609–619.
32. S.B. Wen, X. Mao, R. Greif, and R.E. Russo, *Expansion of the laser ablation vapor plume into a background gas. I. Analysis*, Journal of Applied Physics **101** (2007), no. 2, 023114.
33. B. Zel'dovich and Y.P. Raizer, *Physics of Shock Waves and High-Temperature Hydrodynamic Phenomena*, vol. 1,2, Dover, New York, 2002.